Nonlinear wave-number selection in gradient-flow systems

Hsueh-Chia Chang, Evgeny A. Demekhin,* Dmitry I. Kopelevich, and Yi Ye
Department of Chemical Engineering, University of Notre Dame, Notre Dame, Indiana 46556
(Received 23 September 1996)

The selection of a final periodic state (wave pattern), out of a family of such states, is shown to be governed generically by defects for the lowest order gradient-flow model, the generalized Kuramoto-Sivashinsky equation. Such defects arise when the nonlinear dispersion relationship of the periodic states couples with the flow-inducing Galilean zero mode, in a manner unique to gradient dynamics, to trigger a modulation instability and a self-similar, finite-time evolution toward jumps in the local wave-number gradient and mean thickness. This coupled modulation instability is much stronger than the classical phase modulation instability. The jumps at these defects then serve as wave sinks whose strength relaxes in time. Due to such consumption of wave peaks (nodes) at the relaxing defects, the bulk wave number away from the defects decreases in time until a unique stable periodic state is reached whose speed is equal to its differential flow rate with respect to change in thickness. We estimate the defect formation dynamics and the final relaxation toward equilibrium analytically, and compare them favorably to numerical results. [S1063-651X(97)10003-4]

PACS number(s): 47.54.+r, 47.20.Lz, 47.35.+i, 47.20.−k

I. INTRODUCTION

The translationally invariant, uniform rest state of an extended system is typically unstable to one-dimensional disturbances within a band of wave numbers. These Fourier modes can grow and saturate to form a family of one-dimensional periodic states (rolls or waves). However, only a subset of this family of saturated states are stable, and the final state approached by any initial condition is presumed to lie within this stable band. Considerable effort has hence been expended to determine the stable band, and has led to classical secondary stability criteria for periodic states like the Eckhaus bound for nondispersive systems, the Lange-Newell and Benjamin-Feir criteria for dispersive systems, the Busse balloon, and other two-dimensional stability bounds [1–5] for rolls.

Although a band of periodic states stable to all disturbances can sometimes be found, which member of this subset is eventually selected and the dynamics of the selection process remain unknown, and are active areas of research. Suggested approaches include mean-field theories from phase transition [6,7] which often predict that noise selects a unique periodic state with the lowest energy. However, the presence of a continuum of stable and unstable periodic states, without an obvious functional for minimization, renders such statistical theories difficult and uninformative in the most general case. Recently, it has been established that the large-time dynamics of near-critical extended systems is dominated by local domains (patches) of monochromatic periodic states separated by defects (domain walls or dislocations) [8,9]. Such defects can move as one periodic state expands at the expense of another. Wave-number selection can also proceed as wave-number shocks appear in the bulk area, and propagate toward or away from the defects [10]. The wave number selected is then related to the front selection problem [11,12], since there are many possible wave-number shocks. Insofar as the defects interact and move and serve as sinks and sources of wave-number shocks, their nucleation, interaction, and annihilation then become key steps in the selection of the final periodic state. Nevertheless, it has not been established whether a preferred state is always selected, and there seems to be a multitude of selection processes. Statistically stationary, defect-mediated spatiotemporal chaos can also occur if defects are generated and annihilated continuously, and a uniform periodic state is never reached [13].

The aforementioned theories for extended-domain dynamics are typically described by complex Ginzburg-Landau (CGL) type amplitude equations appropriate for near-critical systems with a narrow band of unstable wave numbers and periodic states, as typified by the well-studied Rayleigh-Bénard instability. It is known for such systems that the nucleation of defects is greatly dependent on the Goldstone mode (drift flow in Rayleigh-Bénard instability) whose dynamics must be coupled to the CGL. At a finite Prandtl number, a periodic state can induce a drift flow within the fluid which can, in turn, compress the local wave number into the unstable region such that the ''stress'' can only be relieved by the formation of a defect. This nucleation process is often modeled by two coupled equations for the phase of the complex amplitude in the CGL (whose gradient is the wave number) and the Goldstone zero mode [14,15]. However, such an analysis usually does not extend beyond numerical simulation. Recently, Charru and Barthelet [16] have also observed defects with jumps in the local film thickness in sheared two-phase flow. These defects then become either wave sinks or wave sources that are the main driving forces behind the wave dynamics. The thickness jumps also underscore the importance of the zero mode in defect dynamics. Exactly how the zero mode couples with the modulation phase instability to produce defects has yet to be elucidated. One approach is to assume that the zero-mode dynamics is slaved to the phase dynamics, and its effect on the latter can be projected by center manifold theory, for example, into higher-

*Permanent address: Dept. of Applied Mathematics, Kuban State Technological University, Krasnodar 350072, Russia.

order terms in the phase equation [17–19]. Defect formation is again demonstrated numerically, but a generic pattern selection process is still not revealed. It is also questionable that the zero mode is a slave mode in light of Charru and Barthelet's observation of ''hydraulic'' jumps at the defects.

To complicate matters, there is an important class of extended-domain systems whose unstable band is not narrow, and the final periodic states can often contain many Fourier modes. They are hence beyond the CGL description. In the limit of large wavelength, the periodic states resemble an array of localized structures (solitary waves or pulses) which contain a large band of Fourier modes. The large bandedness of this class of systems is due to mass conservation, and its dynamics is described by scalar evolution equations of the gradient conservation form

$$\frac{\partial h}{\partial t}=-\frac{\partial}{\partial x}\,q(h,h_x,h_{xx},h_{xxx}). \tag{1}$$

They include thin-film lubrication equations for falling films, evaporating film with Marangoni effects, reaction fronts, sheared films and core-annular flows, etc. [20–27]; Cahn-Hilliard equations for phase transition if concentration is used as an order parameter [28]; liquid jets in air [29]; and others. Because of the gradient operator, the homogeneous state is neutrally stable and, because a long-wave stabilization mechanism does not exist, the unstable band can extend to zero wave number. The same formulation can also be applied to vector gradient-flow evolution equations, but we shall restrict ourselves to the scalar case here. For convenience, we shall adopt the thin-film nomenclature and refer to h as the film height and q the flow rate. Each derivative corresponds to a higher order in the long-wave Benny-type lubrication expansion, and we have truncated the expansion at the fourth derivative.

Although the gradient flow described by Eq. (1) is one dimensional, its region of validity is considerable for most open-flow extended systems it describes. Such hydrodynamic systems often obey some form of Squire's theorem, such that transverse variations are filtered away from small-amplitude noise with a large two-dimensional Fourier content. As a result, at a large distance downstream, the wave patterns are essentially one dimensional with variations in the streamwise direction only. We first note that, unlike the CGL equation, any global uniform state ($h=$const) is a solution to the translationally invariant equation (1) with no x-dependent coefficient. However, mass conservation through the boundary condition stipulates a particular global uniform state which is chosen through scaling and reduction to be the zero state here. Expanding about the zero uniform state and retaining leading-order terms in h (amplitude expansion) and in $\partial/\partial x$ (long-wave expansion), one obtains after proper scaling to remove the maximum number of parameters the following generic evolution equation, the generalized Kuramoto-Sivashunsky (GKS) equation or the Kawahara equation

$$\frac{\partial h}{\partial t}+\frac{\partial q}{\partial x}=\frac{\partial h}{\partial t}+\frac{\partial}{\partial x}\,(2h^2+h_x+\delta h_{xx}+h_{xxx})=0, \tag{2}$$

with a single parameter δ for the dispersion term. A moving-frame transformation is used to eliminate any h_x term. Expansion about nonzero uniform states will only contribute to this removable term, and hence one can expand about the zero state without loss of generality. This is hence the most general weakly nonlinear equation for gradient-flow systems, and it has been the subject of many studies [30–39]. For nondispersive systems with $x\rightarrow -x$ symmetry, δ vanishes exactly, and one obtains the Kuramoto-Sivashunsky (KS) equation. The unique invariance of Eqs. (1) and (2) to a shift in the mean film thickness is due to the gradient form, and this Galilean symmetry is most important in its dynamics. It permits a local thickness variation from zero via a slow modulation instability.

A simple normal mode analysis reveals that the band of unstable wave numbers for the zero uniform state lies within the band $\alpha\in(0,1)$ with a neutral wave number $\alpha_n=1$ and a maximum-growing mode of $\alpha_{\max}=1/\sqrt{2}$. The normal mode analysis also reveals that the phase speeds of these band of unstable modes are

$$\hat{c}(k)=-\delta k \tag{3a}$$

such that the phase speed of the neutral mode is

$$\hat{c}_n=\hat{c}(1)=-\delta. \tag{3b}$$

In an earlier bifurcation analysis [35], we showed that a family of finite-amplitude periodic states with zero average thickness bifurcate supercritically from α_n with speed c_n and zero amplitude into lower wave numbers. This solution branch was traced numerically, and an entire family γ_1 with wavelengths ranging from 2π to infinity was uncovered. In contrast, the narrow band of periodic states for the CGL equation does not extend to states with infinitely long wavelengths. In fact, the large Fourier content of the localized structures in the infinite wavelength limit is beyond the weakly nonlinear, nearly sinusoidal description of CGL-type amplitude equation. In Fig. 1, we subject a high-wave-number member ($\alpha_0=0.9$) of this family for $\delta=1.0$ to a spatially periodic disturbance whose wavelength is much longer than that of the periodic state. The disturbance wave number is $\nu\alpha_0$, with $\nu=0.05$. Consequently, the modulation envelope encompasses about 20 wave peaks. As is evident, the amplitude of the periodic wave and envelope approach zero in finite time at several defect locations where the local wave number α also increases. This compression of waves seems to accelerate the defect formation process. The mean thickness χ jumps discontinuously at the defect, and this jump is further amplified by the compression effect. At a later stage of the dynamics, however, wave compression is so severe at the defects that it actually precipitates peak coalescence such that the net number of waves (nodes or peaks) decreases. The local wave number at the defects also drops precipitously when waves begin to disappear there. This decrease in the wave number at the defect immediately triggers a relaxation process for the jump in the mean thickness, until it becomes almost uniform throughout the domain. During the relaxation, however, the jump defect continues to annihilate waves by coalescence, such that the average wave number over the entire domain decreases monotonically. This dilation process driven by the defect wave sink stops when the χ

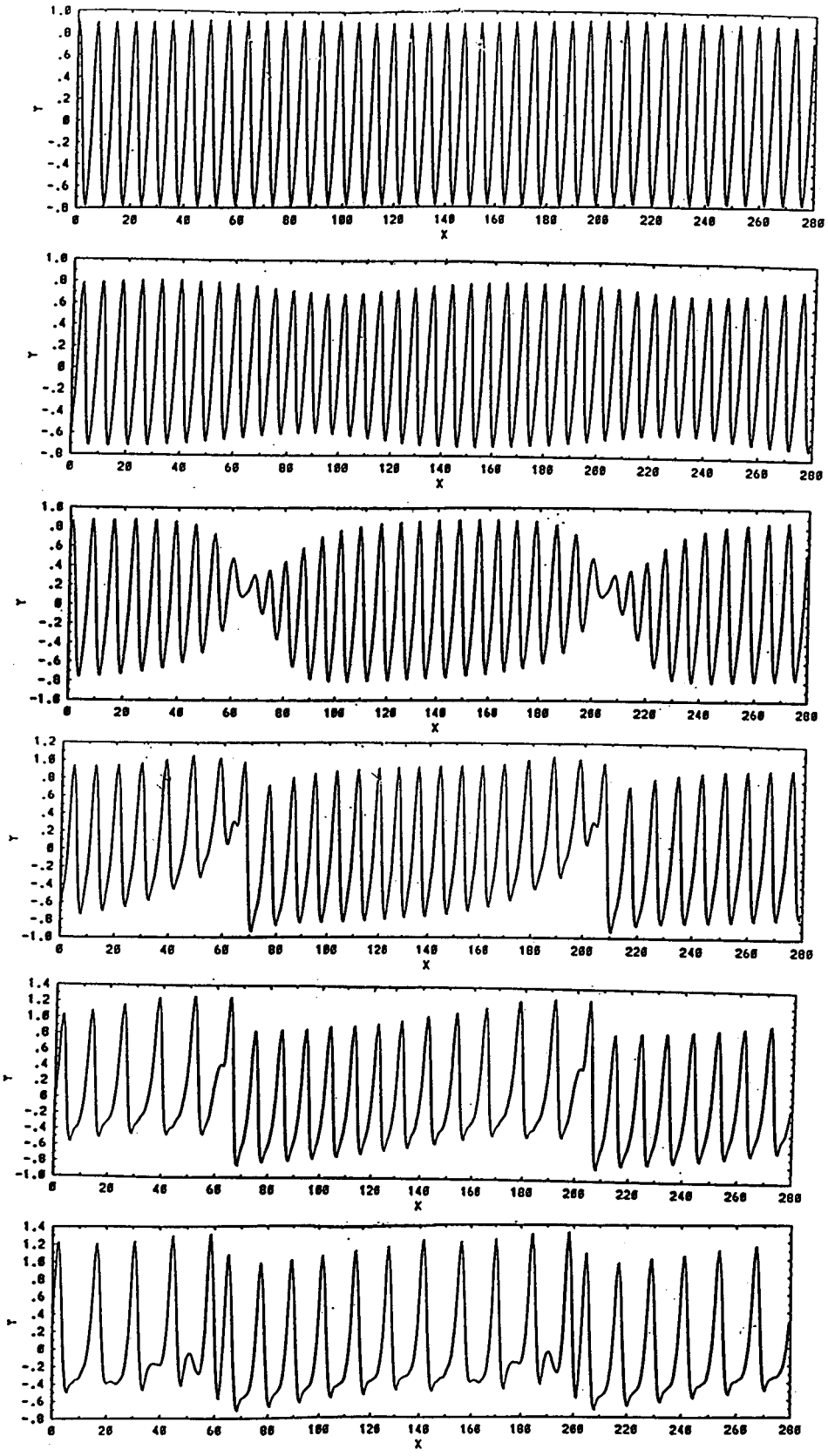

FIG. 1. A zero-mean-thickness periodic state of the γ_1 family of the GKS equation at $\delta=1$, with $\alpha=0.9$, is subjected to a long-wave periodic disturbance with wave number $\nu\alpha$, where $\nu=0.05$. The unstable state evolves toward a stable periodic state with a lower wave number.

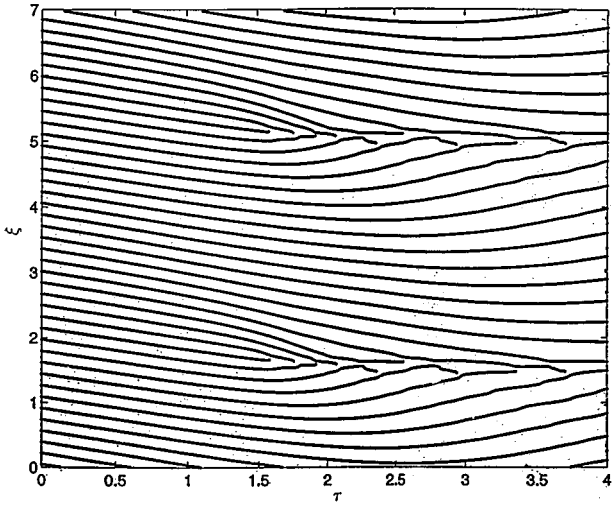

FIG. 2. The peaks of the waves in the simulation of Fig. 1 are traced as world lines. The creation and relaxation of wave-sink defects are evident.

jump of the latter relaxes to zero. An equilibrium wave number α_e is then reached at that point which is much lower than that of the initial periodic state. The amplitude of the final selected state is larger, and its shape begins to take on the localized pulse configuration with a broader Fourier content. The peaks of the individual waves are traced in the world lines of Fig. 2. The formation of a wave sink defect in finite time is evident. We note that the defect moves during the relaxation stage. However, while the initial periodic state travels with a negative speed, the defect relaxes to zero speed, which is also the speed of the final state.

It is clear from the above simulation that the wave-number selection process of the GKS equation is driven by defects in a manner very different from near-critical systems described by the CGL equation. Exploiting the translational and Galilean symmetries of the equation, we shall derive two coupled first-order nonlinear partial differential equations of the gradient or conservation form for the slowly varying wave number α and mean thickness χ. These equations describe the conservation laws for wave nodes (peaks) and mass. They replace the coupled phase-amplitude equations from the CGL formulation with the mean thickness as an explicit representation of the Goldstone mode.

In particular, the classical sideband modulation stability of periodic waves involves a long-wave perturbation of the zero eigenvalue corresponding to the translational invariance at the short scale. The resulting phase diffusion equation, or the higher-order KS equation, describes how the modulation introduces a phase shift relative to the original periodic wave. This approach presumes that the phase dynamics associated with long-wave perturbation of the translational zero eigenvalue is dominant. This phase-dominant theory can only produce defects if higher-order terms in the long-wave modulation expansion and amplitude expansion, from, for example, the projection of the Goldstone zero mode, are included [18,19]. In contrast, we show here that the Galilean invariance of a gradient-flow system introduces an additional zero eigenvalue at short scale, and a second dominant mode for the modulation sideband instability. The translational and Galilean dominant modes will be shown to be coupled to leading order to produce defects (and modulation instability), and are hence much more dominant than a purely phase instability. Moreover, our current theory does not involve an amplitude expansion, and is hence valid for all members of the periodic-wave family up to the solitary pulses. However, due to this extension, unlike the CGL formulation, the speed and ''flow rate'' of the entire family of periodic states must be estimated *a priori*. The coupled equations then describe how the domain is covered by this family of periodic states, and how the family members interact dynamically (and slowly) as governed by node and mass conservation. Most interestingly, we show that a unique final state satisfying a resonance condition is always selected by this mechanism.

A defect forms when a sharp boundary appears between two patches of locally periodic states, and, since the defect escapes our description of slow modulation evolution along the periodic family, its formation corresponds to a blow-up solution to our coupled equations. This is shown to occur in our leading-order expansion in $\partial/\partial x$ whenever the coupled equations, linearized about a particular periodic state, become elliptic with complex eigenvalues. The change of type from hyperbolic to elliptic then offers a very simple criterion for the stability of the states to long modulation disturbances (sideband instability) that is analogous to the Eckhaus and Lange-Newell criteria for the GL and CGL equations. Like the latter, near-neutral states are found to be modulationally unstable.

Unlike the CGL defects, these defects exhibit jumps in the mean thickness χ and the wave-number gradient in the finite-time singularity formation phenomenon shown in Figs. 2 and 6, which we can estimate analytically with a complexification technique. The hydraulic pump in mean thickness χ drives this defect with a speed that is faster than the periodic waves on the lower thickness in front of it, and slower than those on the higher thickness behind it. As a result, these defects act as node sinks, and are very different from the CGL defects. The wave number on either side of the defect hence decreases as wave nodes are consumed, until they become stable to modulation stability. The blow-up behavior for unstable states then works in reverse to relax the jumps until χ is spatially uniform. We are also able to describe this relaxation stage theoretically, and offer an accurate estimate of the final equilibrium wave number when the node annihilation process terminates. This then fully elucidates the generic periodic state selection mechanism for gradient-flow systems. The local dynamics is driven by the modulation instability and evolves along the periodic family from an unstable high wave-number region with small-amplitude sinuous waves to a unique pulselike stable state with larger wavelength and amplitude.

II. PERIODIC FAMILY, SYMMETRY, AND SLOW DYNAMICS

Consider a saturated finite-amplitude, periodic wave H solution to Eq. (2) which propagates at a constant speed C and we choose H such that its mean (average) thickness is zero. Note the distinction between the speed C of the finite-amplitude wave and the phase speed $\hat{c}$ of Eq. (3a) for waves of infinitesimally small amplitude. Then H is described by

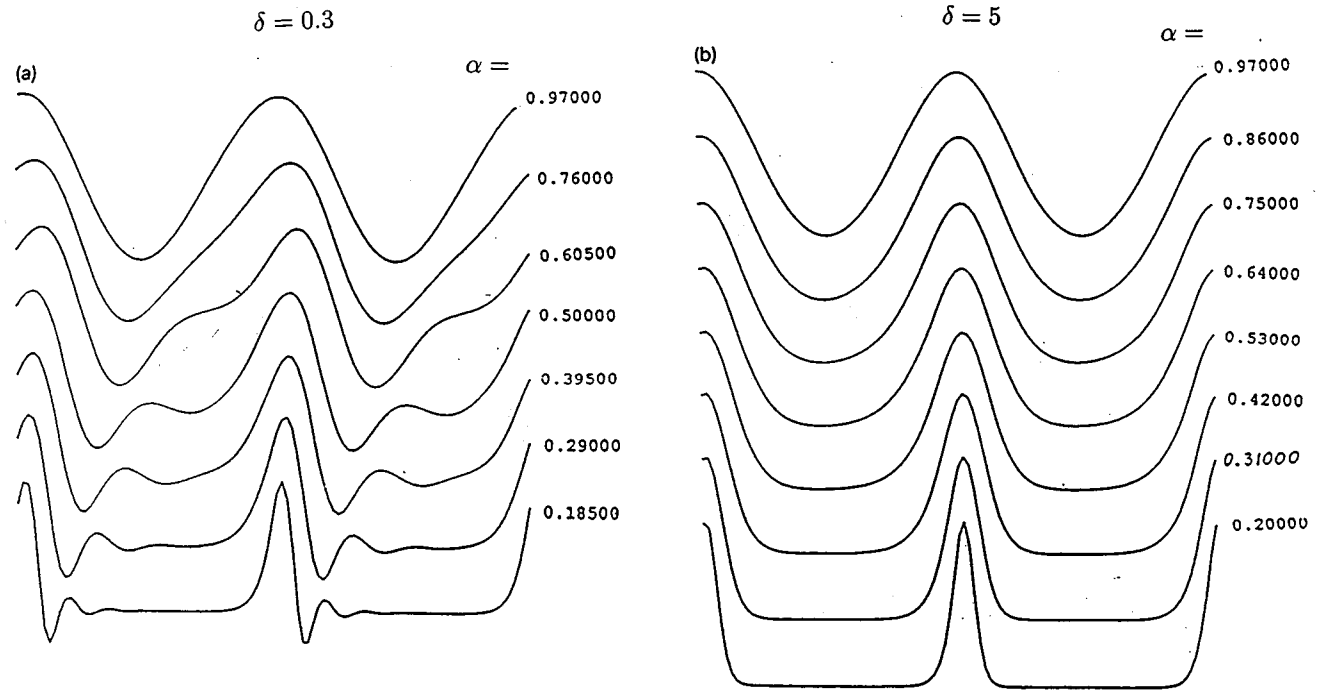

FIG. 3. The γ_1 zero-mean-thickness periodic solutions of the GKS equation at δ=0.3 and 5.0. The horizontal scale has been stretched by $2\pi/\alpha_0$, such that all periodic states have the same scaled wavelength.

$$H''' + \delta H'' + H' - CH + 2H^2 = Q, \tag{4a}$$

$$H(x) = H(x + 2\pi/\alpha), \tag{4b}$$

$$\langle H \rangle = 0, \tag{4c}$$

$$\langle Q \rangle = 2\langle H^2 \rangle, \tag{4d}$$

where Eq. (4a) is in the moving frame with speed C, $2\pi/\alpha$ is the spatial period, Q is the flow rate in the moving frame and $\langle\ \rangle$ denotes integration over one spatial period. A unique feature of these finite-amplitude, zero-mean periodic states is that they have different flow rates Q, and hence can trigger a corresponding change in the film thickness if a distribution of periodic states is present. This is the key mechanism in the modulation instability. The periodic solutions to Eq. (4) for small δ has been estimated by Chang [34], and for large δ by Chang, Demekhin, and Kopelevich [35], Renardy [33], Christov and Velarde [38], and Bar and Nepomnyashchy [39]. Detailed numerical construction has also been carried out by Chang, Demekhin, and Kopelevich [35]. An infinite numbers of solution branches exist at the KS limit of δ=0 due to a Shilnikov bifurcation of the associated homoclinic orbit. However, for δ>1.1, only a single branch γ_1 with α ranging from 1 to zero remains as shown in Figs. 3 and 4. This branch bifurcates from the neutral wave number α_n=1, and represents saturated periodic states from the unstable band of wave numbers. As seen in Fig. 3, the small-α solitary-wave limit of this branch corresponds to localized one-hump pulses.

Near the bifurcation point α=1, a simple Hopf bifurcation analysis of the dynamical system corresponding to Eq. (4) yields, for all δ [35], the speed and flow rate of zero-mean thickness periodic states,

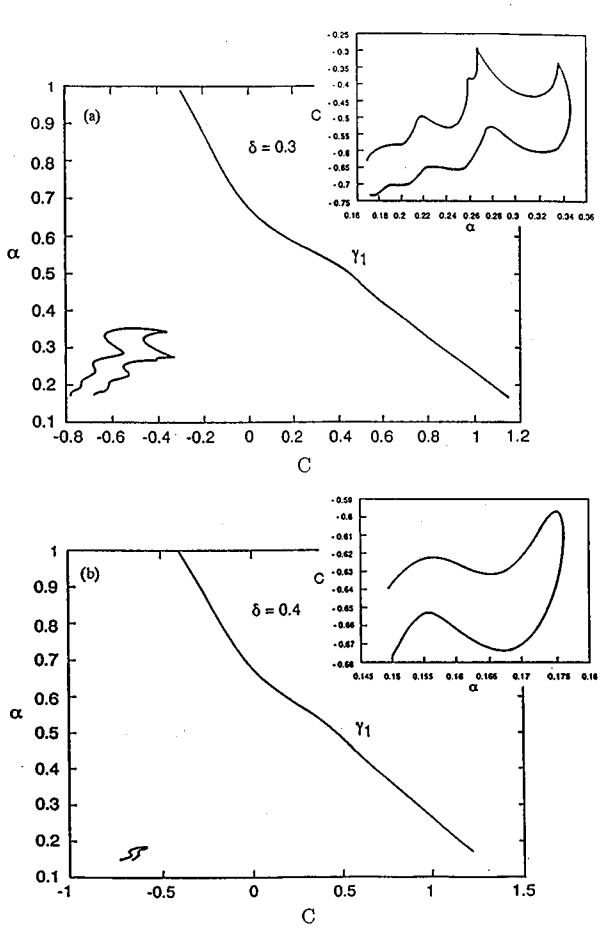

FIG. 4. The γ_1 solution branch for δ=0.3 and 0.4.

$$C(\alpha)\sim 2\delta-3\alpha\delta, \tag{5a}$$

$$\langle Q\rangle(\alpha)\sim\frac{1}{12}(1-\alpha^2)[(4\alpha^2\delta+C)^2+(8\alpha^3-2\alpha)^2]. \tag{5b}$$

We note that these expressions are only valid for $\alpha<1$ since finite-amplitude waves with $\alpha>1$ do not exist. For $\delta\gg 1$, cumbersome elliptic integrals [33,35,39] can also be obtained for C and $\langle Q\rangle$ within the entire range of $\alpha\in[0,1]$. For simplicity, we shall use Eq. (5), and limit ourselves to small-amplitude periodic states with only a few Fourier modes. However, the formulation remains valid for the periodic pulses at vanishing α provided that one contends with the more complex expressions. The variation of the mean flow rate with respect to α in Eq. (5b) immediately suggests that a wave-number gradient can induce flow, and change the local mean thickness from zero due to mass conservation. The change in the local mean thickness, in turn, will be shown to change C, and hence introduce a possible positive feedback mechanism.

It is clear from Eq. (5) that the larger pulselike, low-wave-number members of the zero-mean family travel faster and pack more flow than the smaller harmonic waves with wave numbers near unity. As a result, we expect that a monotonically increasing wave-number distribution with lower wave numbers behind higher ones will steepen in its gradient due to the speed differential. However, this nonlinear dispersion (group velocity) effect is also accompanied by a bulge in the mean thickness due to the concomitant flow gradient. The question is then whether this local increase in film thickness will accelerate (decelerate) the increase in the wave-number gradient, and destabilize (stabilize) the formation of a uniform periodic state. This then involves a study of how a change of the mean thickness from zero will alter the nonlinear dispersion relationship in $C(\alpha)$ and the mean flow rate $\langle Q\rangle(\alpha)$. This feedback effect due to the excitation of the zero mode can even destabilize in the limit of zero amplitude. At this leading order, any wave-number disturbance will not steepen but simply translate without growth if the mean thickness remains zero. However, the phase lag between the excited mean thickness and the initial wave-number perturbation can produce the necessary delay to amplify the gradient of the wave-number disturbance by inducing wave compression and dilation through speed gradients. This is the origin of the modulation instability of a uniform periodic state. At its onset, the disturbances propagate toward each other as the system changes from hyperbolic to elliptic. This growth is then accelerated by the nonlinear mechanism, to form defects with jumps in the wave-number gradient and the mean thickness.

Frisch, She, and Thual [40] reported that the periodic states of the KS equation can suffer the above modulation instability due to a coupling between mean flow and nonlinear dispersion. ''Viscoelastic'' behavior corresponding to oscillations caused by the delay between mean thickness and wave-number gradients in the elliptic region was seen in their numerical simulation. We shall show here that the modulation can evolve further to form the jumps in mean thickness and wave-number gradient, and that such jumps shift the system from an unstable periodic state to a stable one, as seen in Figs. 1 and 2.

The above family of zero-mean periodic family $H(x;\alpha)$ is a one-parameter family parametrized by the wave number α, speed C, or mean flow rate $\langle Q\rangle$. However, any member of this family remains a solution upon a translation in x,

$$x\rightarrow x+\theta,$$

and a Galilean transformation involving a shift in the mean thickness and corresponding corrections to speed and flow rate,

$$H\rightarrow H+\chi, \tag{6a}$$

$$C\rightarrow C+4\chi, \tag{6b}$$

$$\langle Q\rangle\rightarrow\langle Q\rangle-2\chi^2-C\chi. \tag{6c}$$

Since $\langle Q\rangle$ is the flow rate in the moving frame of a viscous falling film with the wall moving in the $-x$ direction with speed C, the flow rate becomes more negative with increasing speed C. The increase in wave speed, on the other hand, is due to the thicker film. For falling films, this is because of the decreased wall drag of thick films which amplifies dispersion. These physical factors account for the Galilean symmetry. We also note that this invariance is only valid up to order H^2 in Eq. (4a). If there exist higher-order terms in H, no transformation in C and $\langle Q\rangle$ can cancel this shift in H even for a gradient-flow system. Hence, the invariance is local in H and is exactly correct only for the leading-order GKS equation.

The above two symmetries imply that there is a three-parameter periodic family with nonzero mean thickness. This family is parametrized by α, θ, and χ. Instead of α, one can also use either $\langle Q\rangle$ or C or a combination of these parameters. We shall assume that the entire domain is covered by members of this three-parameter family, and that the dynamics is driven by slow interaction among its members [41]. As a result, the transformation parameters, α, θ, and χ become slowly varying variables in time and space. Due to variation of the mean thickness parameter χ, the local average thickness of the film also varies in the domain. This feature and the Galilean symmetry in Eq. (6) are unique to gradient-flow evolution and is not found in, say, the CGL dynamics. They are direct results of mass conservation.

The appropriate slow time scale and long length scale will be shown to be

$$\tau=\nu t,\quad \xi=\nu x, \tag{7}$$

where the stretching is carried out with the modulation wave-number ν of the instability. We hence seek solution to Eq. (2) in the stationary frame of the form suggested by symmetry (6)

$$\begin{aligned} h&=H(x,t)+\chi(\xi,\tau),\\ q&=\langle Q\rangle(\xi,\tau)-2\chi^2(\xi,\tau), \end{aligned} \tag{8}$$

where $\chi=\langle h\rangle$ is the mean thickness Galilean zero mode and the omission of the C_χ term in Eq. (6c) is because q is the

flow rate in the stationary frame while Q is its counterpart in the moving frame. The two flow rates are off by a difference of $C\langle H+\chi\rangle$, but the first term has a zero mean and the second cancels the C_χ term in Eq. (6c) to yield Eq. (8). Hence the usual two-scale expansion immediately yields, after integration in the short scale due to the solvability condition, a long-range mass conservation law

$$\frac{\partial \chi}{\partial \tau} = -\frac{\partial q}{\partial \xi} = -\frac{\partial}{\partial \xi}\left(\langle Q\rangle - 2\chi^2\right). \tag{9}$$

The first term within the gradient accounts for flow due to wave-number variation along the zero-mean family, while the second term corrects the flow rate for periodic states with non-zero-mean thickness. Both contribute to the increase in the mean thickness $\langle h\rangle = \chi$. The mean flow $\langle Q\rangle$ is related to the slow varying wave number $\alpha(\xi,\tau)$ through Eq. (5b).

A note of caution about scaling is appropriate here. The GKS equation is usually derived from both a long-wave expansion and an amplitude expansion. In fact, truncation at a particular order leading to the GKS equation assumes a specific relative order between amplitude and $\partial/\partial x$. In this modulation analysis, however, we have only expanded in the long-wave expansion $\partial/\partial\xi$ without a specific amplitude expansion. A relative order is not imposed. As a result, the defect singularities can be smoothed out by higher-order terms in $\partial/\partial\xi$ which should be included when large amplitude and gradient develop at the defects. Nevertheless, singularity formation in finite time does appear at the leading order in $\partial/\partial\xi$, and it offers a dramatic and accurate estimate of the full dynamics except for the local defect-smoothing coalescence events. Fortunately, the coalescence rate is specified by the rate-limiting transfer of waves to the defect, and this transfer mechanism is accurately described by the leading-order $\partial/\partial\xi$ expansion. In any case, since the Galilean invariance is lost beyond second order in amplitude, the large-amplitude, strongly nonlinear dynamics cannot be resolved with a slow modulation theory that expands about the Galilean zero mode.

Returning to our illustrative example of a monotonically increasing spatial wave-number distribution of the zero-mean periodic family, the zero-mean nonlinear dispersion relationship in Eq. (5a) stipulates that the gradient will steepen, but that there will be an accompanying increase in the mean thickness χ in the region of the high-wave-number gradient. This was deduced from the $(\partial/\partial\xi)\langle Q\rangle$ term in Eq. (9). However, the $2\chi^2$ term in the gradient is a nonlinear χ correction, and it shows that the bulge in χ will now steepen in front. Whether this will serve as a positive or negative feedback to the α-steepening effect must be deciphered from the nonzero χ correction to the dispersion relationship.

One can derive more insight by linearizing Eq. (9) about a zero-mean periodic state of wave number α_0 and examining slow varying periodic disturbances to the wave number. For simplicity, we introduce no χ disturbance initially and the spatially periodic wave-number disturbance is stationary. The linearized χ evolution equation (9) receives no contribution form the $2\chi^2$ correction term. Instead, the flow gradient $\langle Q\rangle'(\alpha_0) = (d\langle Q\rangle/d\alpha)(\alpha_0)$ induced by the initial wave-number distribution produces a periodic χ excitation with a $\pi/2$ phase lag relative to the wave-number perturbation, since $\langle Q\rangle'(\alpha_0)$ is negative from Eq. (5b). Because the excited mean thickness can, in turn, induce a growth in the wave-number disturbance, this delay is crucial to the instability of the periodic state.

Deciphering this feedback mechanism and the general evolution of the wavenumber α along the solution branch requires a long-range dispersion relationship involving the speed C of the periodic states. This slow evolution is due to the translational symmetry. The phase representing the shift in the translational invariance is now a slow variable $\theta(\xi,\tau)$. However, since the local solution is required to be a member of the periodic family, we can express θ in terms of a slowly varying α and its frequency ω, which is related to α through the speed relationship (5a),

$$h(\alpha x - \omega t + \theta(\xi,\tau)) = h(\alpha(\xi,\tau)x - \omega(\xi,\tau)t), \tag{10}$$

and we seek variation of h in the form on the right. Let $\phi(x,t;\xi,\tau) = \alpha(\xi,\tau)x - \omega(\xi,\tau)t$, then

$$\frac{\partial \phi}{\partial t} = -\omega, \quad \frac{\partial \phi}{\partial x} = \alpha. \tag{11}$$

The usual two-scale expansion of Eq. (11), using the scalings of Eq. (7), then yield the desired dispersion relationship after cross differentiation,

$$\frac{\partial \alpha}{\partial \tau} + \frac{\partial \omega}{\partial \xi} = 0. \tag{12}$$

This equation describes the conservation law for wave nodes (peaks). In fact, Eqs. (11) and (12) specify the time and space stretching of Eq. (7). Since this dispersion relationship describes finite-amplitude periodic states, the frequency is related to the speed of zero-mean waves in Eq. (5a), after proper correction by Eq. (6) to account for finite mean thickness,

$$\omega = c\alpha = [C(\alpha) + 4\chi]\alpha = \Omega(\alpha) + 4\alpha\chi, \tag{13}$$

where $C(\alpha)$ is the speed of the zero-mean family in Eq. (4a), $\Omega(\alpha)$ its wave frequency, and $c(\alpha,\chi)$ is the speed of a periodic state with wavenumber α and mean thickness χ. The correction to Ω due to a change in the mean thickness χ is then $4\alpha\chi$. This completes the derivation of the coupled slow-evolution equations (9) and (12) for χ and α, respectively.

Since the χ correction for the wave frequency is positive and larger at higher wave number which is generally true for liquid films because thick films enhance dispersion by reducing wall drag on wave motion, it relaxes the steepening of the monotonically increasing wave-number distribution discussed earlier. Hence the χ correction in the mean flow is destabilizing, while the correction for the speed is stabilizing. Which process wins will then be a nonlinear competition between the two effects. Nevertheless, we expect that, if the steepening continues, the mean thickness χ will be steeper (more singular) than the wave number α.

Linearizing Eq. (12) about a zero-mean periodic state with wave number α_0, one notes that, without the $4\alpha\chi$ correction term, any α disturbance would simply translate at a speed of $-\Omega'(\alpha_0)$ without growth. However, coupling with the mean-thickness zero mode contributes a $-4\alpha_0(\partial\chi/\partial\xi)$

term to the growth of the wave-number disturbance. Hence, the $\pi/2$ phase lag between a stationary, periodic α perturbation and the χ excitation it induces can now produce a positive feedback to amplify the wave-number disturbance. More precisely, the α conservation equation (12) stipulates that α will increase (decrease) with a negative (positive) speed or frequency gradient due to wave compression (dilation). The maximum of the induced χ wave has a $\pi/2$ phase lag behind the maximum of the original stationary wave-number disturbance such that the χ gradient is negative at the wave-number maximum. The $4\alpha_0\chi$ term, originating from the Galilean symmetry (6b) as seen in Eq. (13), then stipulates that waves of the same wave number are faster with a higher mean thickness. As a result, the maximum of the wave-number disturbance now experiences a negative speed gradient, and grows as the waves are compressed. Conversely, a minimum will decrease its wave number through wave dilation—the amplitude of the wave-number disturbance will grow. However, we have based our argument on the assumption that the initial wave-number disturbance remains stationary. Actually, it has also translated with a speed of $-\Omega'(\alpha_0)$. As a result, whether the positive feedback through mean-thickness excitation remains destabilizing is determined by a competition between stabilizing dispersion (speed differential between the nonlinear periodic states), represented by the nonlinear ''group velocity'' $\Omega'(\alpha_0)$, and a destabilizing zero-mode excitation, represented by the negative flow gradient $\langle Q\rangle'(\alpha_0)$. The two competing effects are coupled through the $4\alpha_0$ term from Galilean symmetry, which describes how a thicker film accelerates the waves. The physics of the linear modulation instability can be made more clearly by noting that, in the linear limit,

$$\frac{\partial\hat{\alpha}}{\partial\tau}=-\Omega'(\alpha_0)\,\frac{\partial\hat{\alpha}}{\partial\xi}-4\alpha_0\,\frac{\partial\hat{\chi}}{\partial\xi},$$

$$\frac{\partial\hat{\chi}}{\partial\tau}=-\langle Q\rangle'(\alpha_0)\,\frac{\partial\hat{\alpha}}{\partial\xi},$$

where the linearization is about $(\hat{\alpha},\chi)=(\alpha_0,0)$. Combining the two equations yields

$$\hat{\alpha}_{\tau\tau}+\Omega'(\alpha_0)\hat{\alpha}_{\tau\xi}-4\alpha_0\langle Q\rangle'(\alpha_0)\hat{\alpha}_{\xi\xi}=0,$$

which can obviously yield a growing periodic disturbance in $\hat{\alpha}$. The interaction between the nonlinear dispersion term (group velocity) Ω' and nonlinear flow gradient $\langle Q\rangle'$ unique to the present system is also clear. A more explicit derivation of the modulation stability criterion will be offered subsequently. However, it is first noted that if $\langle Q\rangle'$ is zero, $\hat{\alpha}$ never grows. This represents the classical modulation instability with only the phase contribution, and underscores the dominance of current instability when mass flow is permitted. The former is only unstable when the higher-order effects in $\partial/\partial\xi$ are included while the latter is already unstable at the leading order.

We have replaced the slowly varying phase θ by the frequency ω, which is related to α through the nonlinear dispersion relationship (13). This leaves α and χ as the only independent slow variables, and they are described by the two coupled first-order partial differential equations in the slow-evolution equations (9) and (12). It is instructive to compare them to some classical modulation theories. The long-range, nonlinear dispersion relationship (12) appears in many classical phase diffusion theories, but the nonlinear frequency Ω is often only expressed implicitly, and there is also no explicitly derived correction due to the mean-thickness (zero mode) adjustment [10,15,17,18,42]. The zero-mode evolution equation (9), however, is unique to gradient-flow dynamics due to mass conservation. This was first realized by Frisch, She, and Thual [40], who derived a similar set of equations for the KS equation, whose coefficients are determined numerically, from more lengthy multiscale expansion techniques. However, their coupled equations are linear, and hence they offer no further information beyond the onset of modulation instability. The coefficients of Frisch, She, and Thual's coupled equations are derived from a weakly nonlinear amplitude expansion of the same order ν as the time scale and long-wave length scale in Eq. (7). We have confirmed the validity of our slow evolution equation at this resolution by inserting the slow-amplitude expansions (5) into our linearized equations and obtained the same coefficients as Frisch, She, and Thual, albeit that our coefficients are explicit while theirs must be evaluated numerically. It should be emphasized, however, that the current derivation does not involve any amplitude expansion, and hence both the linearized version and fully nonlinear version have higher resolution than the one resulting from an amplitude expansion. The accuracy of our equation with respect to the amplitude is only limited by the accuracy of $\langle Q\rangle(\alpha)$ and $\Omega(\alpha)$ for α far from α_n. These quantities can be estimated numerically if high resolution is required. On the other hand, energy conservation and the corresponding symmetry apply in some integrable systems, and supply another evolution equation missing from our dissipative system. For example, in Whitham's classical modulation theory for deep water waves, there is an equation for slowly varying wave amplitude (energy) that replaces Eq. (9) [43].

Modulation instability occurs for a monochromatic periodic state when mass conservation and nonlinear dispersion conspire to destabilize any wave-number gradient. Linearizing the coupled slow-evolution equations (9) and (12) about a particular zero-mean solution with wave number α_0, one obtains

$$\frac{\partial}{\partial\tau}\begin{pmatrix}\hat{\alpha}\\ \hat{\chi}\end{pmatrix}+\mathbf{A}\,\frac{\partial}{\partial\xi}\begin{pmatrix}\hat{\alpha}\\ \hat{\chi}\end{pmatrix}=0, \tag{14}$$

where

$$\mathbf{A}=\begin{pmatrix}\Omega'(\alpha_0) & 4\alpha_0\\ \langle Q\rangle'(\alpha_0) & 0\end{pmatrix}.$$

The stability of the periodic state with wave number α_0 to long modulations (sideband disturbances) can then be obtained by substituting the Floquet normal mode

$$\begin{pmatrix}\hat{\alpha}\\ \hat{\chi}\end{pmatrix}\sim\mathbf{u}e^{i\xi-\lambda t}=\mathbf{u}e^{\nu(ix-\lambda t)}, \tag{15}$$

where ν is the disturbance wave number, and λ is the eigenvalue of the matrix $i\mathbf{A}$ and is independent of ν,

$$\lambda = i\Omega'(\alpha_0)/2 \pm i\sqrt{D}/2, \tag{16a}$$

$$D(\alpha_0;\delta) = [\Omega'(\alpha_0)]^2 + 16\alpha_0\langle Q\rangle'(\alpha_0). \tag{16b}$$

It is then clear that the periodic state is stable (unstable) to long modulations if Eq. (14) is hyperbolic ($D>0$) or elliptic ($D<0$) respectively. This condition (16) represents the analog of the Echkaus, Benjamin-Feir, and Lange-Newell sideband stability criteria for CGL or nonlinear Schrödinger equations to the present gradient-flow systems. Unlike the purely phase instability of the former systems, the current instability involves both phase (wave number) and Galilean (mean thickness) zero modes. The key physical mechanism, at least at small amplitude, is the delayed excitation of the mean thickness unique to gradient flows. The $16\alpha_0$ term in Eq. (16b) arises from the Galilean symmetry (6b) and its positive sign reflects the fact that waves with higher mean thickness travel faster. This is generally the case for thin falling and sheared films [44,45] as the wall dissipation becomes less retarding to wave motion. As such, any delayed zero-mode excitation will be destabilizing regardless of the dispersion. Hence, the sign of $\Omega'(\alpha_0)$ is unimportant in Eq. (16b), and a necessary condition for instability is that, at the same thickness, the large lower wave-number pulses carry more flow than the small, high-frequency, harmonic waves, viz. $\langle Q\rangle'$ is negative. The sign of $\langle Q\rangle'$ is very much a function of the shape of the periodic states. To leading order for any scalar gradient flow, $\langle Q\rangle = 2\langle H^2\rangle$ as in Eq. (4d) and, for nearly harmonic waves near the neutral wave number $\alpha=1$ with only one or two significant Fourier modes, $\langle Q\rangle'$ is always negative since the wave amplitude grows with decreasing α, which is used as the bifurcation parameter in the Hopf bifurcation analysis. In fact, the near-neutral expression (5b) shows that $\langle Q\rangle'$ becomes less negative as α decreases from unity. Hence we expect near-neutral waves to be more modulationally unstable. If they are indeed unstable, there exists a critical wave number α_c, defined by $D=0$, below which the periodic states are stable. For localized pulses beyond the validity of Eq. (5b), the rate of increase in amplitude must compete against the corresponding increase in speed to specify the stability, as seen in Eq. (16b). This competition is entirely determined by the shape of the waves and, for near-neutral waves, the phase lag between the locked Fourier harmonics [44,45].

In Fig. 5, we favorably compare the upper bound α_c to the stable band of stable periodic states from Eq. (16) to our numerical Floquet stability of the γ_1 zero-mean branch reported in [35]. A simple expansion of Eq. (16) at large δ shows that this stability bound α_c approaches 0.75 as δ approaches infinity. This limit is actually reached very rapidly and, by $\delta=2$, α_c can be accurately approximated by 0.75. Hence periodic states between 0.75 and 1 are unstable to modulation instability at large δ. The slight deviation from the numerical value is due to higher-order corrections in the long-wave expansion (7), since the current theory is only valid to leading order in ν. However, the excellent agreement underscores the fact that the current modulation instability of the periodic states, with dominant coupling with the Galilean mode, is more dominant than the liner and classical phase modulation instability, which only appears in the next order in ν.

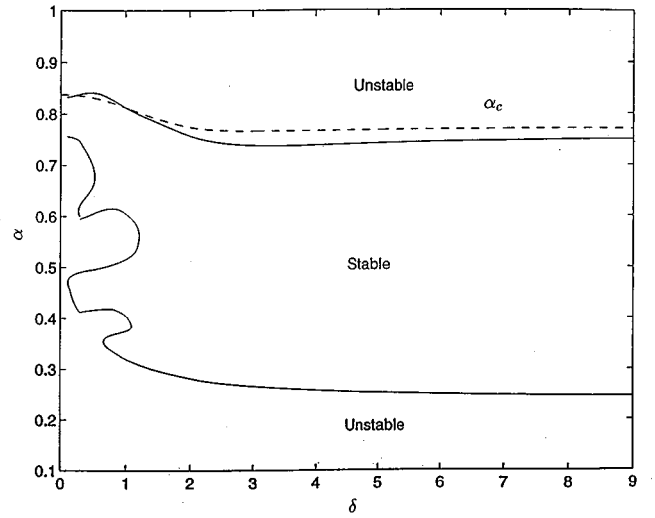

FIG. 5. Comparison of α_c in dotted line from Eq. (16) to a numerical Floquet stability analysis of the γ_1 family. The lower stability bound for the stable band of periodic state arises from a different mechanism [51] beyond the scope of the current theory.

III. SELF-SIMILAR DEFECT FORMATION AND COMPLEXIFICATION

The invariance of the slow-evolution equations in Eqs. (9) and (12) and their linearized version (14) to the transformation $\xi \to a\xi$ and $\tau \to a\tau$ yields a growth rate $-\nu\lambda_r$ in Eq. (16a) that scales linearly with respect to the wave number ν of the modulation disturbance. Since the GKS equation (2) has a quadratic nonlinearity involving one derivative, any fundamental Fourier mode in the wave-number gradient χ_x will excite its overtone in a rapid cascading of energy to higher wave numbers. Due to the quadratic interaction and the linear dependence of the growth rate on the mode number, the amplitude of the nth harmonic of χ_x scales as $\epsilon^n e^{n\mu^0 t}$, where ϵ is the amplitude of the fundamental and μ^0 is its growth rate. Summation of this geometric series immediately shows

$$\chi_x \sim (\epsilon e^{\mu^0 t} - 1)^{-1} \sim (t_f - t)^{-1}, \tag{17}$$

where $t_f \sim -\ln\epsilon$. We hence expect the χ jump to develop in finite time in the manner described by Eq. (17), and with a blow-up time t_f that scales as logarithm of the disturbance amplitude ϵ.

That the singularity formation dynamics is self-similar with a $(t_f - t)^{-1}$ scaling can be verified by a simple manipulation of the slow-evolution equations (9) and (12). These two partial differential equations can be converted into two coupled ordinary differential equations,

$$\eta f' + \frac{\partial\langle Q\rangle}{\partial\alpha}(g)g' - 4ff' = 0,$$

$$\eta g' + \left[\frac{\partial\Omega}{\partial\alpha}(g) + 4f\right]g' + 4gf' = 0$$

by the self-similar transforms

$$\chi = f(\eta), \quad \alpha = g(\eta), \quad \eta = \frac{x}{t_f - t}.$$

For our subsequent numerical scrutiny, we shall show that χ scales linearly in x near the singularity and hence, $\chi = f(\eta) \sim k\eta$ near the singularity at $t \sim t_f$. Consequently, a jump in χ forms with a $(t_f - t)^{-1}$ scaling in time.

We shall confirm this expected finite-time singularity formation both by analyzing the wave dynamics of the GKS equation in Figs. 1 and 2 more carefully, and by integrating the slow-evolution equations (9) and (12). For the latter purpose, we shall adopt the complexification scheme of Garabedian [46], Moore [47], and Caflisch and Orellana [48]. More specifically, Eqs. (9) and (12) in the unstretched x and t coordinates can be written as

$$\frac{\partial}{\partial t}\begin{pmatrix}\alpha\\ \chi\end{pmatrix} + \begin{pmatrix}a_{11} & a_{12}\\ a_{21} & a_{22}\end{pmatrix}\frac{\partial}{\partial x}\begin{pmatrix}\alpha\\ \chi\end{pmatrix} = 0, \tag{18}$$

where the coefficients a_{ij} are functions of α and χ. We then define the left eigenvector $(l^{\pm},1)$ by the eigenvalue problem

$$(l^{\pm},1)\begin{pmatrix}a_{11} & a_{12}\\ a_{21} & a_{22}\end{pmatrix} = a^{\pm}(l^{\pm},1), \tag{19}$$

with eigenvalues $a^{\pm}$ which are real if Eq. (18) is locally hyperbolic, and complex conjugates if elliptic. The characteristics do not possess any geometric meaning in the latter case, but we can still proceed formally. Since the coefficients a_{ij} are not constant, the characteristics are not straight lines, nor are there always simple Riemann invariances along them. Instead, we define a pair of characteristic coordinates (μ,ν) for the characteristic curves as

$$l^{+}\alpha_{\mu} + \chi_{\mu} = 0 \quad \text{along} \quad a^{+}t_{\mu} = x_{\mu}, \tag{20a}$$

$$l^{-}\alpha_{\nu} + \chi_{\nu} = 0 \quad \text{along} \quad a^{-}t_{\nu} = x_{\nu}. \tag{20b}$$

To accommodate the elliptic case with complex conjugates $a^{\pm}$ and $l^{\pm}$, we define another set of coordinates appropriate for the elliptic case,

$$\xi = \frac{\mu + \nu}{2}, \quad \eta = \frac{\mu - \nu}{2i} \tag{21}$$

and transform Eqs. (18) and (20) to

$$\begin{pmatrix}\alpha\\ \chi\\ t\\ x\end{pmatrix}_{\xi} = \frac{1}{\Delta}\begin{pmatrix}\mathbf{B}_1 & 0\\ 0 & \mathbf{B}_2\end{pmatrix}\begin{pmatrix}\alpha\\ \chi\\ t\\ x\end{pmatrix}_{\eta}, \tag{22}$$

where

$$\mathbf{B}_1 = \begin{pmatrix}a_{11} - a_{22} & 2a_{12}\\ 2a_{21} & -(a_{11} - a_{22})\end{pmatrix},$$

$$\mathbf{B}_2 = \begin{pmatrix}a_{11} + a_{22} & -2\\ -2a_{12}a_{21} & -(a_{11} + a_{22})\end{pmatrix},$$

and $\Delta = \sqrt{-(a_{11} - a_{22})^2 - 4a_{12}a_{21}}$. In the elliptic region of interest here, Δ is real and the submatrix $\mathbf{B}_1$ has purely imaginary eigenvalues. The trace of $\mathbf{B}_2$ also vanishes, and it has either a conjugate pair of purely imaginary eigenvalues or two real eigenvalues of opposite sign.

With transformation (21), (x,t) are now expressed as functions of real variables (ξ,η), and, since any function of a characteristic coordinate is still a characteristic coordinate, the one-to-one map implies that (ξ,η) are also functions of (x,t). We have freedom in mapping the initial data at $(x, t=0)$ and we choose

$$\xi(x, t=0) = 0, \quad \eta(x, t=0) = x \tag{23}$$

The key ''trick'' in the complexification scheme is to transform the top decoupled system in Eq. (22),

$$\begin{pmatrix}\alpha\\ \chi\end{pmatrix}_{\xi} = \frac{1}{\Delta}\mathbf{B}_1\begin{pmatrix}\alpha\\ \chi\end{pmatrix}_{\eta}, \tag{24}$$

to a hyperbolic system with real eigenvalues by complexifying η,

$$\eta \rightarrow \eta + i\omega. \tag{25}$$

Assuming χ and α are analytic functions of η such that the Cauchy-Riemann condition holds,

$$\chi^{r}_{\eta} = \chi^{i}_{\omega}, \quad \chi^{r}_{\omega} = -\chi^{i}_{\eta}, \tag{26}$$

where the superscripts denote the real and imaginary parts of χ, as usual. A direct consequence of the Cauchy-Riemann condition is that

$$\chi_{\eta} = (\chi^{r}_{\eta} + i\chi^{i}_{\eta}) = (\chi^{i}_{\omega} - i\chi^{i}_{\omega}) = -i\chi_{\omega}. \tag{27}$$

This reduces Eq. (24) to

$$\begin{pmatrix}\alpha\\ \chi\end{pmatrix}_{\xi} = -\frac{i}{\Delta}\mathbf{B}_1\begin{pmatrix}\alpha\\ \chi\end{pmatrix}_{\omega}, \tag{28}$$

such that $i\mathbf{B}_1$ has two real eigenvalues of opposite signs, and the system is now hyperbolic with orthogonal characteristics in the ξ-ω plane. If $\mathbf{B}_2$ in the lower decoupled system has purely imaginary eigenvalues, we also render it hyperbolic by transforming $\partial/\partial\eta$ to $-i(\partial/\partial\omega)$. Otherwise, $\mathbf{B}_2$ has real eigenvalues of opposite sign, and the hyperbolic lower system can be solved in the ξ-η coordinates of Eq. (22).

Although α and χ are strictly complex numbers after complexification, we shall only be interested in their values along the real η axis which also satisfy Eq. (28). We can then trace (α,χ) and (x,t) as functions of (ξ,η) by using the usual characteristic methods. However, the tradeoffs in this complexification scheme are that the initial data cannot be conveniently mapped into the ξ-ω plane by Eqs. (23) and (25) and the extra calculation introduced by one more dimension of the complex variable.

If

$$\alpha(x, t=0) = \alpha_0(x), \tag{29}$$

which can be analytically continued, it can be transformed to

$$\alpha(\eta + i\omega, \xi = 0) = \alpha_0(\eta + i\omega), \tag{30}$$

and hence the α (or χ) is parametrized by $\eta(=x)$ at $\xi=0$.

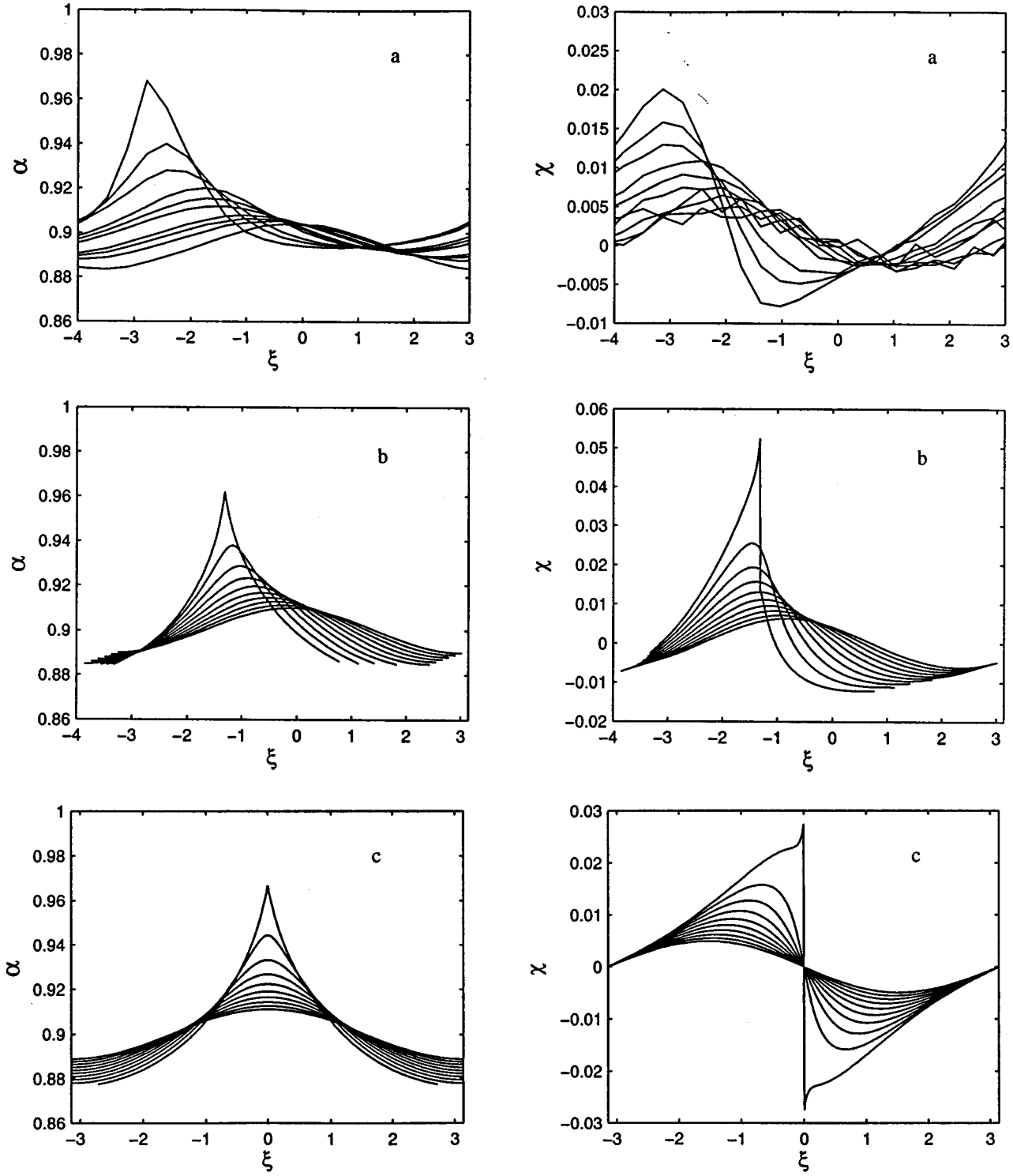

FIG. 6. Comparison of locally averaged α and χ profiles from Fig. 1 by direct numerical simulation of the GKS equation (a) to those obtained from the coupled slow-evolution equation (b) for $\delta=1$. The symmetric α profiles and antisymmetric χ profiles for $\delta=0$ from the slow-evolution equations are shown in (c).

We hence need to solve the hyperbolic system (28) and the lower decoupled system for (x,t) for all possible values of η in the ξ-ω plane. We follow the orthogonal characteristics until ω vanishes. From transformation (25), the values of (x,t,α,χ) at this point of penetration are true values of Eq. (22), and hence Eq. (18), before complexification. We have successfully implemented this scheme to solve the slow-evolution equation. As we shall demonstrate, this approach can even offer analytical results for the case with small-amplitude initial data.

In Fig. 6(a), we locally average the α and χ profiles from the simulation of Fig. 1. For $\delta=1$, the α profile shows the

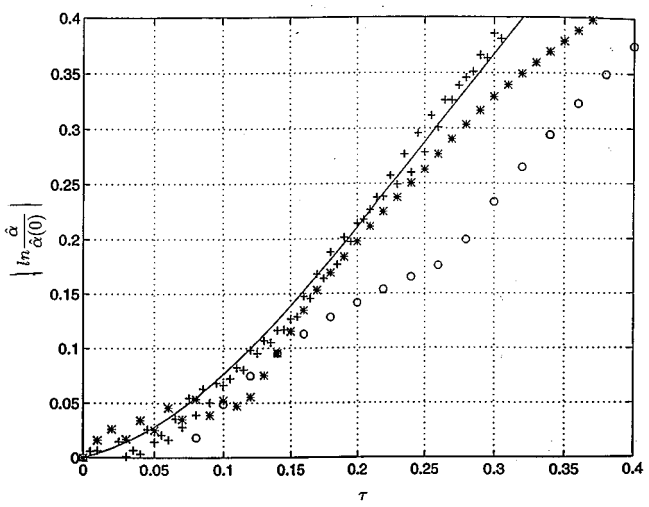

FIG. 7. Comparison of the singularity formation stage from the GKS equation and the slow-modulation equations. Solid line: slow-modulation equations; +: GKS equation with $\nu=0.05$; *: GKS equation with $\nu=0.1$; ○: GKS equation with $\nu=0.2$.

formation of an asymmetric cusp, while the χ profile seems to jump. As seen from Fig. 6(b), these features are reproduced by integrating Eqs. (9) and (12) for the same conditions in Fig. 1. Excellent quantitative agreement is also evident.

We have also examined the self-similar cascading to successive overtones with linearly increasing growth rates by integrating both the GKS equation and the slow-evolution equations for a periodic state ($\alpha=0.9$) perturbed by periodic modulations of varying wave number ν and amplitude $\hat{\alpha}(0)$. According to our theory, the growth in $\hat{\alpha}$ at a particular location scales as $\hat{\alpha}(0)e^{\nu\mu_0 t}$ or $\hat{\alpha}(0)e^{\mu_0\tau}$, where $\tau=\nu t$. Hence $\ln|\hat{\alpha}/\hat{\alpha}(0)|$ should be independent of ν and $\hat{\alpha}(0)$ used in the simulation of the GKS equation. The measured $\hat{\alpha}$ is the local wave number, where the singularity will form and its evolution reflects the wave compression during singularity formation, seen also in the world lines of Fig. 2. The solution of the slow-evolution equation is also shown in Fig. 7. Due to its invariance to a stretching transformation in both x and t, the collapse is exact, and only a single curve results. More interesting is that the linear increase in $\ln[\hat{\alpha}/\hat{\alpha}(0)]$ vs τ ceases when quadratic interaction excites the overtone 2ν. As is evident in Fig. 7, this linear inception region is followed by another linear region whose slope is twice as large. This is also because the overtone has twice the growth rate of the fundamental. It is this continuous doubling of the growth rate as the overtones are excited that leads eventually to finite-time formation of jumps in χ and α_x anticipated in Eq. (17).

We have postulated before that the formation time t_f of these singularities scales as $-\ln\epsilon$, where ϵ is the disturbance amplitude. This formation time can actually be estimated analytically for $\delta=0$. For this KS equation, Eqs. (9) and (12) can be written more explicitly in the original (x,t) coordinates

$$\frac{\partial}{\partial t}\begin{pmatrix}\alpha\\ \chi\end{pmatrix}+\begin{pmatrix}4\chi & 4\alpha\\ \langle Q\rangle'(\alpha) & -4\chi\end{pmatrix}\frac{\partial}{\partial x}\begin{pmatrix}\alpha\\ \chi\end{pmatrix}=0, \tag{31}$$

where $\langle Q\rangle'(\alpha)=(144\alpha^5+2\alpha-36\alpha^3-128\alpha^7)/3$ is the negative flow gradient. The general complexification scheme can be simplified here by using

$$x\to x+iy, \quad \chi\to\chi+i\beta. \tag{32}$$

Actually, it can be shown that the defect always forms at $x=0$ for the KS equation at $\delta=0$, and for the initial disturbances we adopt later. As a result, Eq. (32) can be further simplified if one needs only to know the evolution at $x=0$,

$$x\to iy, \quad \chi\to i\beta. \tag{33}$$

Transformation (33) immediately reduces Eq. (31) to

$$\frac{\partial}{\partial t}\begin{pmatrix}\alpha\\ \beta\end{pmatrix}+\begin{pmatrix}4\beta & 4\alpha\\ -\langle Q\rangle'(\alpha) & -4\beta\end{pmatrix}\frac{\partial}{\partial y}\begin{pmatrix}\alpha\\ \chi\end{pmatrix}=0 \tag{34}$$

which is hyperbolic whenever Eq. (31) is elliptic because of the change in the sign of $-\langle Q\rangle'(\alpha)$. Restricting ourselves to a specific initial disturbance with only one harmonic with amplitude ϵ,

$$\alpha_0=1+\epsilon\cos x, \quad \chi_0=\epsilon\sin x,$$

we can also complexify it to

$$\alpha_0=1+\epsilon\cosh y, \quad \beta_0=\epsilon\sinh y,$$

Two characteristic lines of the hyperbolic system (34) emanate from every initial point at $t=0$. They are defined by

$$\frac{d}{dt}y_\pm=\pm\sqrt{16\beta^2-\tfrac{4}{3}\langle Q\rangle'(\alpha)\alpha}. \tag{35}$$

We can solve for the characteristics explicitly by substituting the solution of linearized version of Eq. (34) into Eq. (35) and collect up to $O(\epsilon)$ terms. Here we just take y_+ characteristic lines, although the y_- characteristics behave in a similar manner. The y_+ characteristic lines can be resolved to first order in the disturbance amplitude ϵ as

$$y_+(y_0,t)=y_0+\sqrt{24}t+4\epsilon f(t)\cosh y_0,$$

where y_0 is the origin of the characteristic at $t=0$ and

$$f(t)=\frac{25}{3}\left(\frac{1}{2}\sinh\sqrt{24}t-\frac{1}{\sqrt{6}}\cosh\sqrt{24}t+\frac{1}{\sqrt{6}}\right).$$

Singularities form when two y_+ (or y_-) characteristic lines cross, and they are first observed along the limiting curve to which other characteristic lines converge tangentially. A condition for tangency is then $dy_+/dy_0=0$, which specifies y_0 and, hence, y_+. However, the singularity at this tangency appears in the real plane only when $y_+=0$ such that x is not a complex number. The defect singularity is then formed at t_f defined by

$$\ln\left(\frac{3}{25\epsilon}\right)=\ln\left(\frac{\sinh\sqrt{24}t_f}{2}-\frac{\cosh\sqrt{24}t_f}{\sqrt{6}}+\frac{1}{\sqrt{6}}\right)+\sqrt{24}t_f+1, \tag{36}$$

which can be inverted for small ϵ to yield

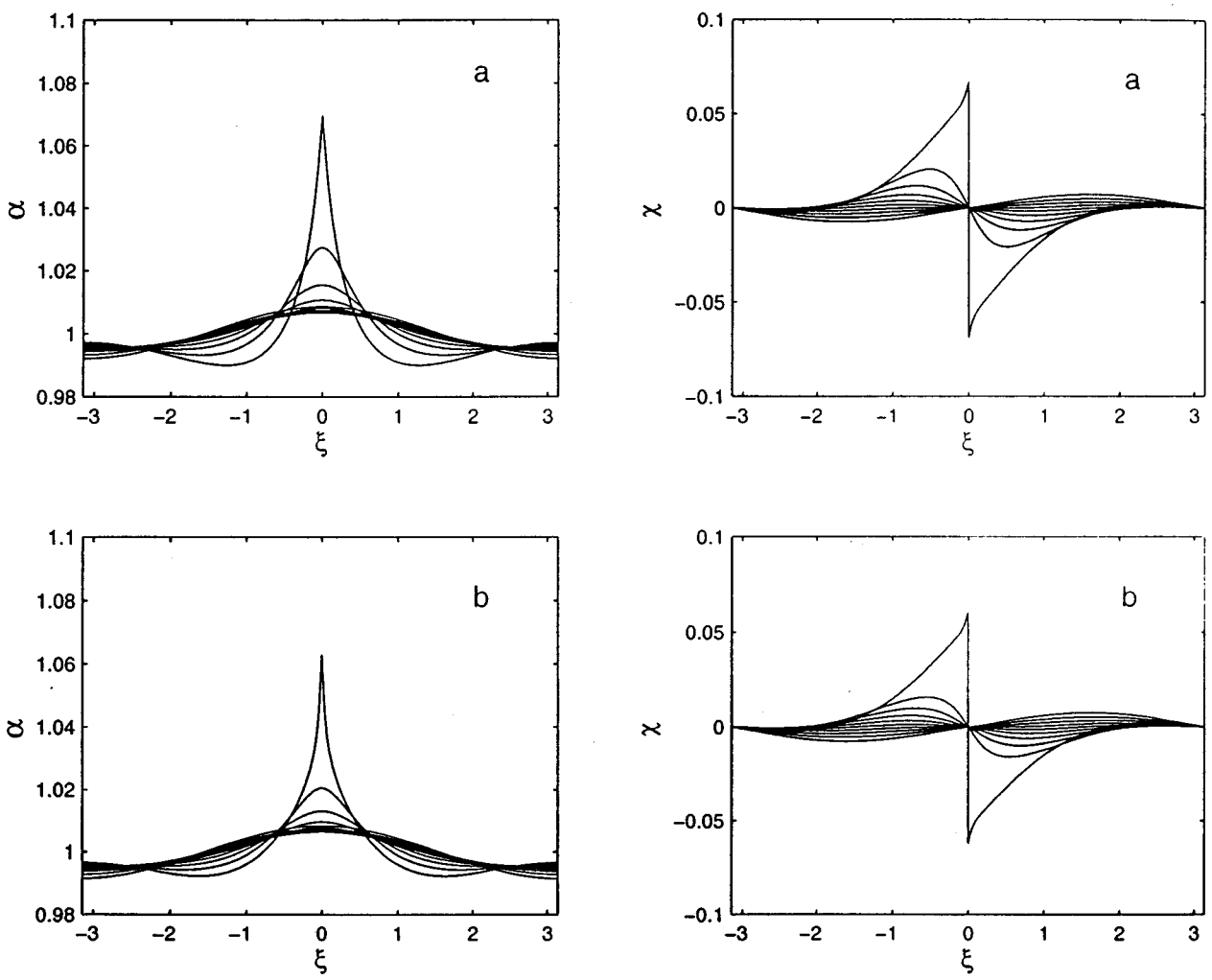

FIG. 8. (a) Analytical estimate of the α and χ evolution for the initial data $\alpha=1+\epsilon\cos x$ and $\chi=\epsilon\sin x$ at $\delta=0$. (b) Simulated version of (a) from the slow-evolution equation. The agreement with the analytical result is excellent.

$$t_f\sim-\ln\epsilon, \tag{37}$$

as is consistent with our postulate. By comparing Eq. (37) to our numerical results from the slow-evolution equations, we find it offers an excellent estimate despite its simplicity.

In fact, for the KS equation with $\delta=0$, the simplicity of the complexification scheme leading to Eq. (34) allows us to estimate the Riemann invariants to the leading order along each characteristic line $y_\pm$ from the initial data explicitly,

$$I_\pm=\alpha\beta+\frac{\sqrt{6}}{2}\left(-\frac{22}{3}\,\alpha+\frac{25}{6}\,\alpha^2\right),$$

such that the values of α and β as functions of t and y can be written in closed form, albeit rather complicated ones, after the complexification transform (32) valid for all x. It implies that shock profile can be estimated. In Fig. 8, we favorably compare this analytical result to the numerical solution of the slow-evolution equation.

For the general case of $\delta\neq0$, the complexification estimates are still possible, but not as simple as before. Explicit estimates are also very cumbersome to derive. Nevertheless, one still sees singularity formation time scaled as $-\ln\epsilon$, cusp formation in α, and a jump in χ for all values of δ. One distinct feature is that the singularity is no longer symmetric with respect to x, and shifts back and away from $x=0$ as seen in Figs. 6(a) and 6(b).

IV. JUMP RELAXATION

The singularity formation process described in Sec. III leads to jumps in χ and α_x in finite time. The maximum α at the singularity is actually pushed toward the neutral wave number $\alpha_n=1$, where there are no finite-amplitude periodic states beyond α_n. This is clearly seen in Figs. 1, 6, and 8, and it is also evident that the local wave amplitude decreases to zero. Away from the singularity, α is dilated to below α_c into the hyperbolic region. While severe wave-field compression and dilation occur during the jump formation stage, the number of wave peaks remains the same. Wave annihilation only begins after the jump is formed and, in fact, begins to relax its amplitude. As seen from the world lines of Fig. 2, the singularity quickly evolves into a wave sink whose speed is lower than the wave speed behind it and higher than the wave speed in front. Waves with decreasing amplitude are then sucked into the sink on both sides. This precipitates a

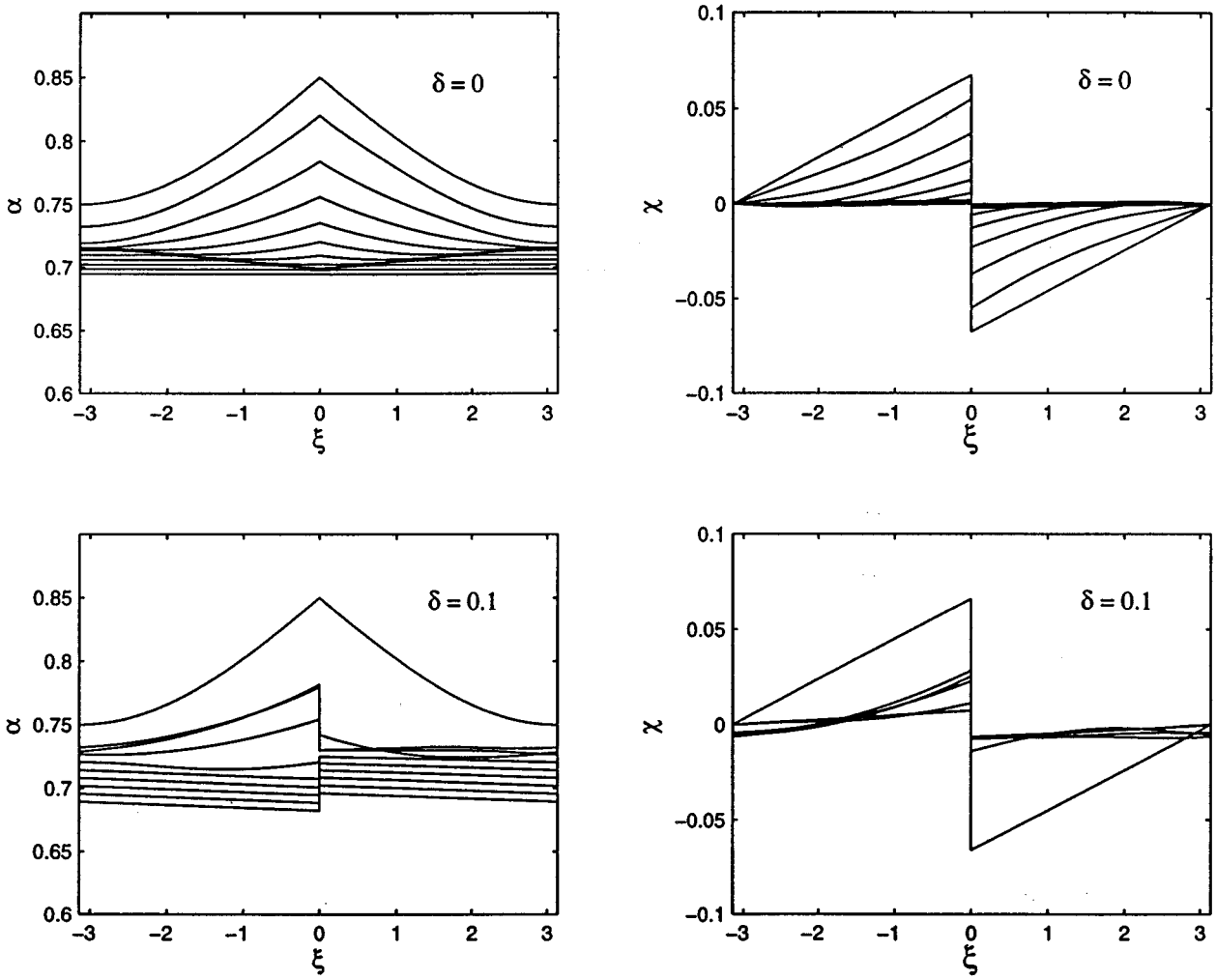

FIG. 9. Jump relaxation from the simulation of the slow-evolution equation with initial data $\alpha=0.85-0.1\cos((x-\pi)/2)$ and $\chi=0.0235(x-\pi)$ for $\delta=0$ (time step: 0.3) and with initial data $\alpha=0.85-0.1\cos((x-\pi)/2)$ and $\chi=0.021(x-\pi)$ for $\delta=0.1$ (time step: 1.2). Relaxation to a uniform $\chi_e=0$ and $\alpha_e=0.66$ is evident.

dramatic drop in the local wave number at the singularity that cannot be captured by our slow-evolution equations which are valid over the stretched long scales and for small amplitudes. Both the coalescence event at the singularity and the dilation effect away from it then push the entire α distribution below α_c very rapidly. In Fig. 2, for example, the singularity forms at $\tau_f=\nu t_f=1.5$ and by $\tau=2.0$, the entire distribution is below $\alpha_c=0.89$ for the corresponding $\delta=1$ as seen in Figs. 5 and 10. From Fig. 2, it can be seen that the wave number at the singularity remains the highest even when the entire distribution has entered the stable hyperbolic region. Moreover, the χ jump is not at all affected by the coalescence. The nonlinear coupling that serves to steepen the α and χ distributions to form singularities now acts to relax this χ jump.

Since we do not know the exact α and χ profiles created by coalescence, we have integrated the slow-evolution equations with some arbitrary profiles resembling the profiles from the GKS solution at this stage. They have a cusp in α and a jump in χ. As seen in Fig. 9, such profiles with the α distribution below α_c relax to a uniform α distribution α_e and a uniform zero χ distribution. We note that for all conditions, an exact solution over one period to our slow-evolution equations exist and have the unrealistic forms

$$\alpha=\alpha_0(1-4bt),$$
$$\chi=b(x-x_0)/(1-4bt), \tag{38}$$

where α_0, b, and x_0 are arbitrary constants. This solution will eventually lead to a negative wave number, because the equation is not cognizant of the fact that C and $\langle Q\rangle$ in Eq. (5) are limited to a wave number between 0.5 and 1. Our numerical scheme will sometimes pick up Eq. (38) after the equilibrium $(\alpha(x),\chi(x))=(\alpha_e,0)$ is reached. We simply ignore this numerical artifact since it corresponds to shock steepening.

The singularity relaxation process is also distinct for $\delta=0$ and $\delta>0$. The asymmetry with respect to x that exists during the formation stage in Figs. 6(a) and 6(b) for $\delta>0$ persists during the relaxation stage. The singularity hence continues to shift as seen in Fig. 9. Moreover, a jump in α can also develop for $\delta>0$, such that the front side of the cusp actually slips down relative to the back one. An α jump is hence

created to accompany the χ jump. Both jumps then decay to zero at equilibrium, with α approaching a uniform equilibrium value α_e, and χ approaching zero due to mass conservation.

After the shocks are formed, the characteristics converge and there are certain domains on the x-t or ξ-τ plane that cannot be reached by characteristics emanating from the initial data at t (or τ)=0. To determine the values of α and χ in these domains, we need to track the shocks, and impose conservation laws across them. Some of these laws, like wave peak balance, arise naturally from the governing equations while others, like mass conservation, must be imposed externally. It is the mass conservation law that will allow us to estimate the shock speed, and hence track the shocks to the next time step. In fact, the α and χ values at the jump can then be estimated for the next time step from an expression we shall derive. These values at the shock could then serve as boundary values which, in conjunction with the initial data, can then specify the α and χ values for the entire domain at the next time step. Characteristics from the shocks can reach domains that are not accessible to characteristics from the initial data. The α and χ values at the shocks must be estimated at every time step, as the shock speed is determined from the distributions at a given time. Other than providing the necessary boundary conditions for our numerical scheme, the conservation laws, especially the natural ones, also provide invaluable information about the dilation dynamics. We shall first derive a natural node conservation law, and then impose the mass conservation law to estimate shock speed.

The net global dilation rate due to the consumption of the waves by the relaxing singularity and the final equilibrium wave number α_e can actually be estimated from global mass and wave conservation. Let $N=\int_0^L \alpha d\xi$ be the total number of waves (peaks or nodes) over a periodic domain of size L containing a relaxing singularity. Integrating the α evolution equation (12) over the domain then yields, from the Liebnitz rule,

$$\frac{dN}{d\tau}=\int_0^{s_-}\alpha_\tau d\xi+\int_{s_+}^{L}\alpha_\tau d\xi-\dot{s}(\alpha_+-\alpha_-)=\Delta\omega-\dot{s}\Delta\alpha, \tag{39}$$

where $\dot{s}$ is the speed of the singularity, subscripts $\pm$ denote values after and before the jump and Δ the change across the jump, $\Delta\omega=\omega_+-\omega_-$, and $\Delta\alpha=\alpha_+-\alpha_-$. Since the nonlinear frequency ω is just $c\alpha$, one obtains

$$\frac{dN}{d\tau}=-\alpha_-(c_--\dot{s})-\alpha_+(\dot{s}-c_+), \tag{40}$$

and it simply states that the wave annihilation rate is determined by the differential between the wave speed and the defect speed on both sides of the jump. Note that both quantities in the brackets of Eq. (26) must be positive, because a local dilation process occurs at the jump, and a wave source is formed if they are negative. The present formulation cannot handle a wave source, since the finite-amplitude waves require some transient period and length to grow to finite amplitude. Without a proper description of the wave generation mechanism, the jump must relax to zero the instant c_- is smaller than c_+. Hence the entire jump relaxation process cannot extend beyond equilibrium. The ''entropy'' condition

$$c_->\dot{s}>c_+$$

must be satisfied for all time.

A similar integral of the χ evolution equation (9) yields

$$\frac{\partial}{\partial\tau}\int_0^L\chi d\xi=\Delta q-\dot{s}\Delta\chi. \tag{41}$$

However, if we impose the physical constraint that the total amount of liquid $\int_0^L\chi d\xi$ must remain constant, one immediately obtains the shock speed

$$\dot{s}=\frac{\Delta q}{\Delta\chi}. \tag{42}$$

Hence, given the α and χ distributions at a given time, the shock location at the next time step can be estimated from Eq. (42). However, for the shock to serve as boundaries for our numerical scheme, such that domains inaccessible to characteristics emanating from the initial data can be reached, the $\alpha_\pm$ and $\chi_\pm$ values at the shock must be determined. To this end, we note that

$$\frac{d\alpha_\pm}{d\tau}=\frac{\partial\alpha_\pm}{\partial\tau}+\frac{\partial\alpha_\pm}{\partial\xi}\dot{s}=-\frac{\partial\omega_\pm}{\partial\xi}+\frac{\partial\alpha_\pm}{\partial\xi}\dot{s}.$$

Hence, by evaluating all the ξ derivatives on both sides of the shock and using Eq. (42), we can update $\alpha_\pm$ for the next time step. Similarly, $\chi_\pm$ can be estimated by

$$\frac{d\chi_\pm}{d\tau}=\frac{\partial\chi_\pm}{\partial\tau}+\frac{\partial\chi_\pm}{\partial\xi}\dot{s}=-\frac{\partial q_\pm}{\partial\xi}+\frac{\partial\chi_\pm}{\partial\xi}\dot{s}.$$

We use these values of $\alpha_\pm$ and $\chi_\pm$ at the shock locations, in conjunction with the α and χ distributions away from the shock, to determine the distributions at the next time step.

As the shock relaxes (α approaches the uniform equilibrium distribution α_e and χ approaches zero), α_+ and α_- must both approach α_e, while c_+, c_-, and $\dot{s}$ should approach each other such that the wave consumption process stops. This immediately yields a resonance condition for the equilibrium wave number and the equilibrium speed of the jump,

$$\lim_{\tau\to\infty}\dot{s}=c(\alpha_e,\chi=0)=C(\alpha_e)=\left(\frac{\partial q}{\partial\chi}\right)_{\chi=0}(\alpha_e), \tag{43}$$

viz. the wave speed should equal the differential flow relative to a change in χ. For the current system, $(\partial q/\partial\chi)_{\chi=0}$ vanishes exactly from Eq. (8), and one concludes that the final defect speed vanishes. From the speed expression (5a),

$$\alpha_e=\tfrac{2}{3}. \tag{44}$$

That the speed of the jump singularity approaches zero is clear from the world lines of Fig. 2, and, in Fig. 10, we depict the change in the number of world lines in the GKS simulation of Fig. 2 as a function of time and show an approach to $\alpha_e=\frac{2}{3}$. We have also verified the validity of Eq. (40) by inserting the values of $\alpha_-=0.94$, $\alpha_+=0.94$,

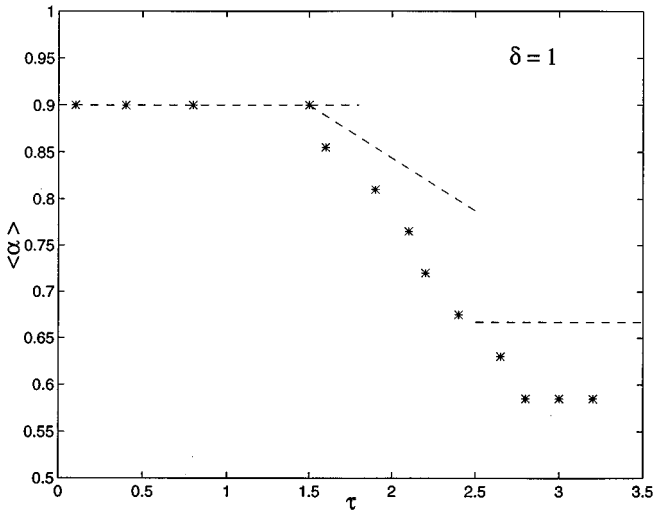

FIG. 10. The average wave number within the domain of simulation of the GKS equation in Fig. 1. The predicted initial wave node consumption rate at the beginning of the relaxation process from Eq. (40) is shown. The parameters $\alpha_-=0.94$, $\alpha_+=0.94$, $\chi_-=0.03$, and $\chi_+=0.005$ are obtained from a simulation of the formation process with the slow-evolution equations. Relaxation to an equilibrium wave number is also evident. The slight deviation of the equilibrium number from $\frac{2}{3}$ is due to the annihilation of one additional peak. This is quite remarkable, considering the small number of peaks between defects and the irregular spacing at the end of evolution.

$\chi^+=0.03$, and $\chi^-=0.005$ estimated from the complexification scheme at the instant of singularity formation at $\tau_f=1.5$. As is evident in Fig. 10, it accurately estimates the initial wave consumption rate as the singularity relaxes.

V. SUMMARY

Unlike near-critical CGL systems, which have a narrow unstable band and which do not respect mass conservation, we have shown here that wave-number selection for a gradient-flow system is a unique mechanism, and that there is a specific preferred wave number α_e defined by Eq. (44). This is because the χ Galilean zero mode of these systems can couple with nonlinear dispersion to leading order to trigger the formation of a jump defect that annihilates waves as it decays. The defect can only relax to zero amplitude when the surrounding wave number has been dilated to α_e. Mass conservation, however, is a generic physical property that must be obeyed by many systems described by the CGL equation. It has, however, been removed in the latter's derivation [17,44]. This is an omission that can obscure the true wave-number selection mechanism, since the current coupled mechanism is far more dominant as it enters in the leading order of the modulation stretching in Eq. (7). Nor is it sufficient to introduce the zero mode as a slave mode to the phase dynamics of the CGL equation, as is often done for the Goldstone drift mode. We are currently extending the CGL formulation to include the zero-mode dynamics.

We also note that the current theory pertains to the selection of a periodic state, but that the asymptotic state at the end of the modulation instability may not be even locally periodic, as seen in the simulation of GKS equation in Fig. 1. In fact, the pulselike structures at this stage often have irregular and discontinuous separation and amplitude as residual effects of the noise-induced, defect-driven dynamics. The final pulse created by coalescence at the jump before it relaxes completely, for example, is typically much larger than the others, as seen in Fig. 1. These localized structures interact individually instead of through a collective modulation instability. The resulting dynamics cannot then be analyzed by assuming local periodicity, and the slow-modulation description through γ_1 periodic waves becomes inappropriate. In earlier papers [49,50], we showed that, for some systems, the current periodic state selection process can be followed by another one involving individual pulse coalescence, such that the number of pulses can decrease further. Such coalescence can also be derived by a coupled amplitude-phase equation, but the amplitude now corresponds to the amplitude of a single pulse and its phase separation from the neighboring pulses. The subsequent dynamics then takes on a distinctly localized feature involving individual pulses. The coarsening process hence may continue beyond the modulation instability, and the final average pulse spacing can be much longer than $2\pi/\alpha_e$, the ''periodic'' state selected by the modulation instability.

ACKNOWLEDGMENTS

This work is supported by a NSF grant and a NASA grant. Y.Y. is grateful for financial assistance from the Center for Applied Mathematics at Notre Dame. We would also like to thank D. T. Papageorgiou for sharing his preliminary work and for informing us of the complexification method.

[1] W. Eckhaus, J. Mech. **2**, 153 (1963).
[2] C. B. Lange and A. C. Newell, SIAM J. Appl. Math. **27**, 441 (1974).
[3] T. B. Benjamin and J. E. Feir, J. Fluid Mech. **27**, 441 (1974).
[4] F. H. Busse, Rep. Prog. Phys. **41**, 1929 (1978).
[5] P. Manneville, *Dissipative Structures and Weak Turbulence* (Academic, Boston, 1990).
[6] Y. Pomeau and P. Manneville, J. Phys. (Paris) Lett. **40**, 609 (1979).
[7] H. R. Schober, E. Allroth, K. Schroeder, and H. Müller-Krumbhaar, Phys. Rev. A **33**, 567 (1986).
[8] P. Coullet, C. Elphick, L. Gil, and J. Lega, Phys. Rev. Lett. **59**, 884 (1987).
[9] N. Bekki and K. Nozaki, Phys. Lett. **110A**, 133 (1985).
[10] P. Coullet, L. Gil, and J. Lega, Physica D **37**, 91 (1989).
[11] W. van Saarloos and P. C. Hohenberg, Physica D **56**, 303 (1992).
[12] E. Ben-Jacob, H. Brand, G. Dee, L. Kramer, and J. S. Langer, Physica D **14**, 348 (1985).
[13] P. Coullet and J. Lega, Europhys. Lett. **7**, 511 (1988).
[14] H. S. Greenside, M. C. Cross, and W. M. Coughran, Phys. Rev. Lett. **60**, 2269 (1988).

[15] A. Pocheau, J. Phys. (Paris) **50**, 2059 (1989).
[16] P. Barthelet and F. Charru (private communication).
[17] M. Cheng and H.-C. Chang, Phys. Fluids A **2**, 1364 (1990).
[18] H. Sakaguchi, Prog. Theor. Phys. **84**, 792 (1990).
[19] A. A. Nepomnyashchy, Europhys. Lett. **31**, 437 (1995).
[20] A. A. Nepomnyashchy, Mech. Zidek. Gaza **3**, 28 (1974).
[21] S. P. Lin, J. Fluid Mech. **63**, 417 (1974).
[22] Y. Kuramoto and T. Tsuzuki, Prog. Theor. Phys. **55**, 356 (1976).
[23] G. I. Sivashinsky, Acta Astron. **6**, 569 (1979).
[24] H.-C. Chang, Chem. Eng. Sci. **41**, 2463 (1986).
[25] C.-A. Peng, L. A. Jurman, and M. J. McCready, Int. J. Multiphase Flow **17**, 767 (1991).
[26] A. P. Hooper and R. Grimshaw, Phys. Fluids **28**, 3 (1985).
[27] D. R. Papageorgiou, C. Maldrelli, and D. S. Rumshitzki, Phys. Fluids A **2**, 340 (1990); A. L. Frenkel, Europhys. Lett. **18**, 583 (1992).
[28] H.-C. Chang, Phys. Fluids **29**, 3142 (1986).
[29] H. C. Lee, IBM J. Res. Dev. **18**, 364 (1974).
[30] J. Topper and T. Kawahara, J. Phys. Soc. Jpn. **44**, 663 (1978).
[31] T. Kawahara, Phys. Rev. Lett. **51**, 381 (1983).
[32] T. Kawahara and S. Toh, Phys. Fluids **31**, 2103 (1988).
[33] M. Renardy, Theor. Comput. Fluid Dynamics **4**, 95 (1992).
[34] H.-C. Chang, Phys. Fluids **29**, 3142 (1986).
[35] H.-C. Chang, E. A. Demekhin, and D. I. Kopelevich, Physica D **63**, 299 (1993).
[36] H.-C. Chang, E. A. Demekhin, and D. I. Kopelevich, Phys. Rev. Lett. **75**, 1747 (1995).
[37] D. M. Alfaro and M. C. Depassier, Phys. Lett. A **184**, 184 (1994); R. D. Benguria and M. C. Depassier, Phys. Rev. A **45**, 5566 (1992).
[38] C. I. Christov and M. G. Velarde, Physica D **86**, 323 (1995).
[39] D. E. Bar and A. A. Nepomnyashchy, Physica D **86**, 586 (1995).
[40] U. Frisch, Z. S. She, and O. Thual, J. Fluid Mech. **168**, 221 (1986).
[41] C. Elphick and E. Meron, Phys. Rev. A **40**, 3226 (1989).
[42] A. C. Newell, in *Propagation in Systems far From Equilibrium*, edited by J. E. Wesfreid *et al.* (Springer-Verlag, Berlin, 1988), p. 122.
[43] G. B. Whitham, J. Fluid Mech. **22**, 273 (1965); Proc. R. Soc. London Ser. A **283**, 238 (1965); **299**, 1456 (1967).
[44] M. Cheng and H.-C. Chang, Phys. Fluids **7**, 34 (1995).
[45] M. Sangalli, M. J. McCready, and H.-C. Chang, Phys. Fluids **9**, 1 (1997).
[46] P. R. Garabedian and H. M. Lieberstein, J. Aero. Sci. **25**, 109 (1958).
[47] D. W. Moore, Proc. R. Soc. London Ser. A **365**, 105 (1979).
[48] R. E. Caflisch and O. Orellana, SIAM J. Math Anal. **20**, 293 (1989).
[49] H.-C. Chang, E. A. Demekhin, and E. N. Kalaidin, J. Fluid Mech. **294**, 123 (1995).
[50] H.-C. Chang, E. A. Demekhin, E. N. Kalaidin, and Y. Ye, Phys. Rev. E **54**, 1467 (1996).
[51] H.-C. Chang, E. A. Demekhin, and E. N. Kalaidin, Physica D (to be published).